# Influence of Air Gap Thickness in Transverse Flux Permanent Magnet (TFPM) Generators for Wind Turbine Application

Maxime R. Dubois, *Member, IEEE*, Henk Polinder, *Member, IEEE*, and Jan A. Ferreira, *Member, IEEE*

***Abstract*—The use of Transverse-Flux Permanent Magnet (TFPM) machines with flux concentration, as direct-driven wind turbine generator is investigated. The ability of TFPM structures with flux-concentration to reduce the cost of active material is looked upon more closely. The Cost/Torque characteristics of TFPM (Transverse-Flux Permanent Magnet) machines and RFPM (Radial Flux Permanent Magnet) machines are presented. It is emphasized how the air gap thickness plays a dominant role in the cost savings provided by the TFPM structure. For air gap thickness below 3 mm, the TFPM structure with flux concentration shows interesting cost benefits, over the RFPM machine. Above the 3.5 mm threshold, TFPM with flux concentration hardly shows any cost advantage over the RFPM structure.**

*Index Terms*—Permanent Magnet Machines, Transverse-Flux Machines, Wind Energy.

## I. Nomenclature

| | |
|---|---|
| $A_{Cus}$ | cross-section of one conductor in the slots |
| $b_s$ | stator slot width |
| $B_1$ | Fundamental component of the no-load flux density |
| $B_{Fesat}$ | Saturation flux density of laminated iron |
| $B_g$ | no-load flux density in the air gap |
| $B_r$ | remanent flux density |
| $d$ | overlap distance between stator core and flux concentrator |
| $E$ | rms no-load voltage |
| $f$ | electrical frequency in Hz |
| $F_m$ | PM equivalent magnetomotive force (mmf) |
| $F_s$ | peak value of the stator magnetomotive force |
| $F_{smax}$, | maximum value of Fs obtained at saturation |
| $g$ | air gap thickness |
| $h_m$ | magnet thickness |
| $h_s$ | stator slot height |
| $h_{sw}$ | height of stator winding in TFPM |
| $h_w$ | thickness of the stator slot wedge |
| $I$ | rms nominal phase current |
| $J$ | current density in the conductors |
| $k_{mag}$ | RFPM ratio of magnet width over pole pitch |
| $k_{sfill}$ | slot filling factor |
| $k_{ws}$ | skewing factor |
| $K_{TFPM\_Cost}$ | TFPM cost advantage factor |
| $l_s$ | length of the stator stack of laminations |
| $l_f$ | length of flux concentrator in axial direction |
| $l_{sw}$ | width of stator winding in TFPM |
| $L_a$ | stator inductance for rotor in aligned position |
| $L_u$ | stator inductance for rotor in unaligned position |
| $m$ | number of phases |
| $n_p$ | number of turns per pole per phase |
| $p$ | number of pole pairs |
| $P_{mech}$ | mechanical power on the machine shaft |
| $r_g$ | air gap radius |
| $R_m$ | PM recoil reluctance |
| $R_g$ | air gap reluctance |
| $R_{stat\_teeth}$ | reluctance of the stator teeth |
| $R_{stat\_yoke}$ | reluctance of the stator yoke |
| $R_{rot\_back}$ | reluctance of the rotor back iron |
| $R_{side}$ | TFPM reluctance of leakage path between stator core and flux concentrator in unaligned position |
| $R_{up}$ | TFPM reluctance per pole pair seen by the stator conductors in unaligned position |
| $R_{ap}$ | TFPM reluctance per pole pair seen by the stator conductors in aligned position |
| $R_{Ccore}$ | reluctance of TFPM stator core on winding side |
| $R_{SScore}$ | reluctance of TFPM stator core on opposite side |
| $R_{LEC}$ | reluctance of leakage path between two adjacent flux concentrators |
| $R_{ctc}$ | TFPM reluctance of leakage path between stator core and adjacent flux concentrator in aligned position |
| $T$ | average continuous torque |
| $w_m$ | magnet width in TFPM machine |
| $w_{sc}$ | TFPM stator core width |
| $w_{rc2}$ | width of flux concentrators |
| $\Phi_g$ | RFPM no-load flux in the air gap |
| $\Phi_{pnl}$ | TFPM no-load flux per pole in the stator core |
| $\Phi_{ps}$ | flux component created by the stator current in the |

This work is supported in part by Delft University Research Institute DU-WIND, and the FCAR (Quebec, Canada).

M. R. Dubois is with Delft University of Technology, The Netherlands, Mekelweg 4, 2628 CD Delft (telephone: (+31) 015 278 6016, e-mail: m.dubois@ its.tudelft.nl).

H. Polinder, is with Delft University of Technology, The Netherlands, Mekelweg 4, 2628 CD Delft (telephone: (+31) 015 278 1844, e-mail: h.polinder@ its.tudelft.nl).

J.A. Ferreira is with Delft University of Technology, The Netherlands, Mekelweg 4, 2628 CD Delft (telephone: (+31) 015 278 6220, e-mail: j.a.ferreira@ its.tudelft.nl).

| | |
|---|---|
| | core of a salient TFPM machine |
| $\Phi_{psat}$ | saturation flux in one pole of stator core of TFPM machine |
| $\Phi_{ptot}$ | sum of no-load flux and stator-created flux in one pole of the stator core of TFPM machine |
| $\mu_{rm}$ | PM recoil relative permeability |
| $\mu_{rFe}$ | relative permeability of laminated steel |
| $\tau_p$ | pole pitch |
| $\theta$ | phase angle between $E$ and $I$ |
| $\omega$ | electrical angular frequency in rad/s |
| $\Omega$ | machine angular rotational speed in rad/s |

## II. Introduction

WIND energy is an increasing percentage of the total energy supplied to the public electricity network. Annual growth rates of 30 % in the number of wind turbines installed have been observed during the last years. To a certain extent, this strong growth rate is helped by the states environmental policies and tax incentives. However, another determining factor has certainly been the decreasing production costs of wind energy [1]. Wind energy is now almost competitive with other more traditional sources of electrical energies, like coal, gas and nuclear generation [2]. Technology development is certainly one of the key factors, in making wind energy more and more cost effective and reliable.

One of the technological advances of the last years concern the use of a direct-drive synchronous generator to replace the conventional gearbox-induction generator combination. The direct-drive technology brings many advantages over the geared-drive technology, like higher reliability and less frequent maintenance. However, the available direct-drive technology is still more expensive than the geared-drive technology [3]. This is one of the reasons why direct-drive wind turbines nowadays occupy only about 10% of the wind turbine market.

The direct-drive wind turbine normally uses a synchronous generator, and a power electronics converter, which is connected to the grid. From these two components, the synchronous generator is the most expensive. In such a context, is there any specific generator technology, which could substantially reduce the cost of the direct-drive generator? The direct-drive wind turbines available today mainly use a conventional synchronous machine with an electrically-excited wound rotor. The replacement of the wound-rotor by permanent magnets (PM) has been studied in [4],[5], and although some gain is perceived, the overall difference in cost remains small, mainly due to the high specific cost of PM material.

This paper investigates how the Transverse-Flux Permanent Magnet (TFPM) machine can further reduce the costs of active material. The costs of active material in both the TFPM machine with flux-concentration and Radial-Flux Permanent-Magnet (RFPM) machines are compared. Both machine types are modeled and optimization programs are developed, which select the designs with the lowest cost/torque ratio for a given generator diameter.

Section IV of this paper describes how the two machine structures are mathematically modeled. In section V, the two machine types are optimized with respect to cost/torque, and the advantage factor of the TFPM machine over the RFPM machine is presented. It will be shown that the thickness of the air gap strongly affects the advantage factor. The last section will explain why the TFPM machine performances depend so much on the air gap thickness.

## III. Machine Structures Investigated

TFPM machines make possible the use of short pole pitches in combination with high current loading. In most TFPM machine prototypes built, this gives very high torque/mass, which also leads to a reduction in the cost of active material. Among the several variants of the TFPM concept, the TFPM machine with double-sided air gap and flux-concentration is chosen for this investigation. This structure was proposed by [6], and is shown in fig. 1. As described in [7], TFPM structures with flux-concentration make a better use of the PM material, and have higher air gap flux density than the TFPM machines with surface magnets.

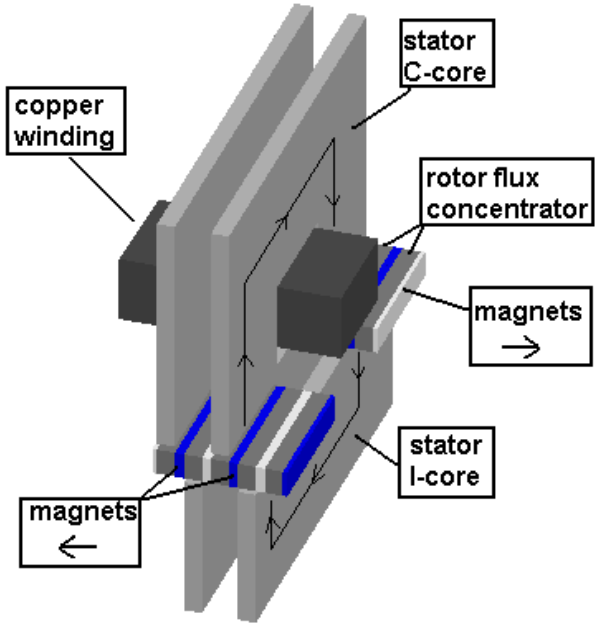


Fig. 1. TFPM machine with flux-concentration. Linear representation.

This TFPM structure is chosen, because it was the first TFPM structure with flux-concentration proposed in the literature, and from which all other TFPM structures with flux-concentration (as in [8]) are derived. The conclusions of this paper will apply to most of TFPM machines with flux-concentration.

The second machine structure analyzed in the paper is the RFPM machine, shown in fig. 2.

## IV. Mathematical Models

The RFPM and TFPM machines are compared on the basis

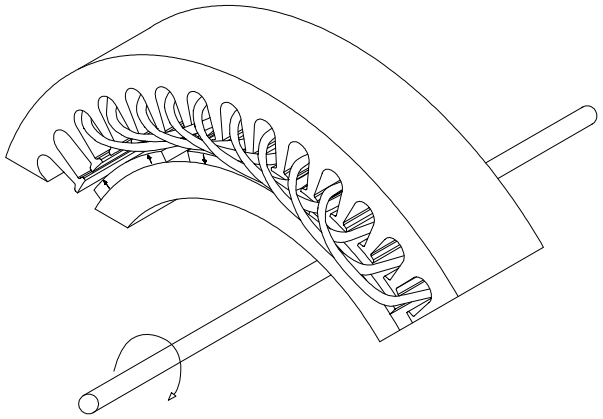

Fig. 2. RFPM machine.

of their cost/torque performances.

The two machine types have a large number of geometrical parameters, which can be varied independently, giving out millions of different design possibilities for a same torque. To identify the design with the lowest cost/torque, a computer program has been developed for the two machine types. The programs predict the machine torque and cost for each set of geometrical parameters, and allow these geometrical parameters to vary within a certain range.

*A. Cost/Torque ratio*

The criterion Cost/Torque is used. The cost of active material is computed by weighting each material with a given specific cost:

- specific cost of laminated steel = 6 Euro/kg
- specific cost of copper = 6 Euro/kg
- specific cost of PM = 40 Euro/kg
- specific cost of powdered iron = 6 Euro/kg

*B. RFPM machine: analytical model*

The optimization program predicts the torque performance for the RFPM machine, from its geometrical parameters. The machine torque $T$ is derived from (1).

$$T = \frac{P_{mech}}{\Omega} \cong \frac{mEI\cos\theta}{\Omega} \tag{1}$$

where the no-load voltage and the phase current are assumed as sinusoidal. $E$ is derived by using (2) and (3), as obtained from a 2-D finite element calculation by [9].

$$E = \frac{8}{\sqrt{2}}\pi k_{ws} B_1 r_g l_s f \tag{2}$$

$$B_1 = \sqrt{2}B_g\left[0.81 - 0.3\frac{(h_m + g)}{\tau_p}\right] \tag{3}$$

Equation (3) is valid for $k_{mag}$ = 0.7. This value has been used in the calculations.

In (2), the stator is assumed as skewed, and $k_{ws}$ is set to 0.95 in the program. The value of $B_g$ is obtained by assuming the magnetic field as traveling in straight lines in the air gap and in the magnets, through the magnetic circuit illustrated in fig. 3.

$$B_g = \frac{\Phi_g}{l_s \tau_p k_{mag}} \tag{4}$$

$\Phi_g$ is derived from the magnetic circuit of fig. 3. In the calculation of $R_{stat\_teeth}$, $R_{stat\_yoke}$, $R_{rot\_back}$ , a constant $\mu_{rFe}$ was used and the machine has been assumed to work below saturation.

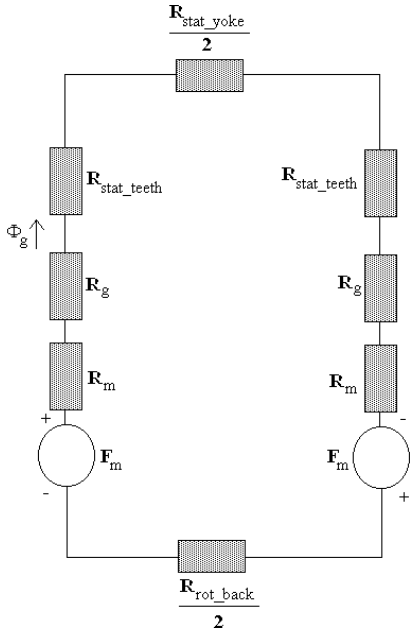


Fig. 3. Magnetic circuit used to determine $B_g$.

The nominal phase current $I$ is calculated with (5) and (6).

$$I = JA_{Cus} \tag{5}$$

$$A_{Cus} = k_{sfill}\frac{\left[b_s(h_s - h_w)\right]}{n_p} \tag{6}$$

In the calculations, the following values are used:

- $J$ = 4.0 A/mm2
- $k_{sfill}$ = 0.5
- $m$ = 3
- $h_w$ = 5 mm
- slot depth/slot width ($h_s/b_s$) = 4
- slot width/tooth width = 1.05
- $B_r$ = 1.23 T
- $\mu_{rFe}$ = 1000
- $\mu_{rm}$ = 1.09
- $B_{FEsat}$ = 1.9 T
- $\theta$ = 0 degree

### C. TFPM machine: analytical model

The TFPM machine is essentially a single-phase machine. It is possible to turn it into a three-phase machine, by stacking three TFPM machines, and shifting their rotors by 120°. The torque of a single-phase machine with salient poles can be expressed as:

$$T \cong \frac{EI}{\Omega}\cos\theta + \frac{\pi I^2 f(L_u - L_a)}{2\Omega}\sin 2\theta \tag{7}$$

where the no-load voltage and the phase current are assumed as sinusoidal, and where the stator inductance is assumed as varying sinusoidally with the electrical angle, between two values $L_a$ and $L_u$.

Expression (7) is written as a function of the global electrical quantities $E$, $I$, $L$, $f$, $\Omega$. We can also derive an expression for $T$, as a function of the local polar quantities:

$$T = \frac{p^2}{2} F_s \left[ \Phi_{pnl}\cos\theta + \frac{F_s}{4}\left(\frac{1}{R_{up}} - \frac{1}{R_{ap}}\right)\sin 2\theta \right] \tag{8}$$

The values of $\Phi_{pnl}$ and $R_{ap}$ are calculated from the magnetic circuit of fig. 4.

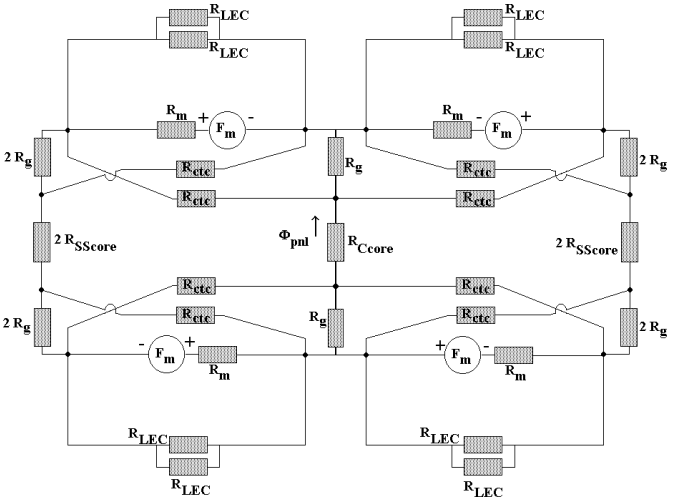


Fig. 4. Magnetic circuit used to determine $\Phi_{pnl}$ *and* $R_{ap}$

In the TFPM machine with flux-concentration and double air gap, the pole pitch is generally short. This makes the flux calculation extremely complex, due to the different leakage paths directed in all 3 dimensions. Each of the lumped reluctances of fig. 4 represents an individual local flux path or leakage path of the total flux. These local flux paths and leakage paths are also shown in fig. 5.

The values of $\Phi_{pnl}$ *and* $R_{ap}$ are obtained by solving the magnetic circuit of fig. 4, which gives:

(9)

$$\Phi_{pnl} = \frac{F_m(R_{ctc} - 2R_g)}{R_m R_g + 2R_{ctc}\left(2\frac{R_g R_m}{R_{LEC}} + R_g + \frac{R_m}{4}\right) + \left(R_{Ccore} + R_{SScore}\right)\left(\frac{2R_m R_g + R_m R_{ctc}}{R_{LEC}} + R_g + R_m + \frac{R_{ctc}}{2}\right)}$$

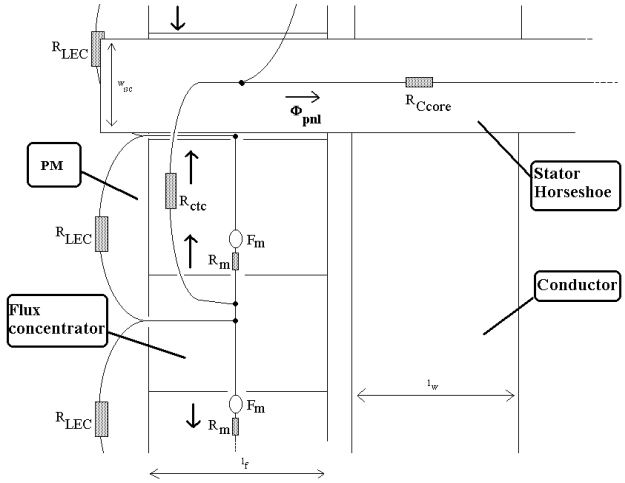


Fig. 5. Top view of the TFPM machine with flux concentration and double-sided air gap, shown in the aligned position. Only one side of the rotor is shown, with the different flux paths replaced by lumped reluctances.

$$R_{ap} = R_{Ccore} + R_{SScore} + R_{T12} + \frac{(R_{T2} + R_{ctc})(R_{T1} + 2R_g)}{R_{T1} + R_{T2} + R_{ctc} + 2R_g} \tag{10}$$

where

$$R_{T1} = \frac{R_{ctc} R_m R_{LEC}}{(R_{ctc} + 2R_g)(2R_m + R_{LEC}) + R_m R_{LEC}} \tag{11}$$

$$R_{T2} = \frac{2R_g R_m R_{LEC}}{(R_{ctc} + 2R_g)(2R_m + R_{LEC}) + R_m R_{LEC}} \tag{12}$$

$$R_{T12} = \frac{2R_{ctc} R_g}{R_{ctc} + 2R_g + \dfrac{R_m R_{LEC}}{2R_m + R_{LEC}}} \tag{13}$$

The magnetic circuit in the unaligned position is simpler. Fig. 6 shows the only possible path for the flux created by the stator winding.

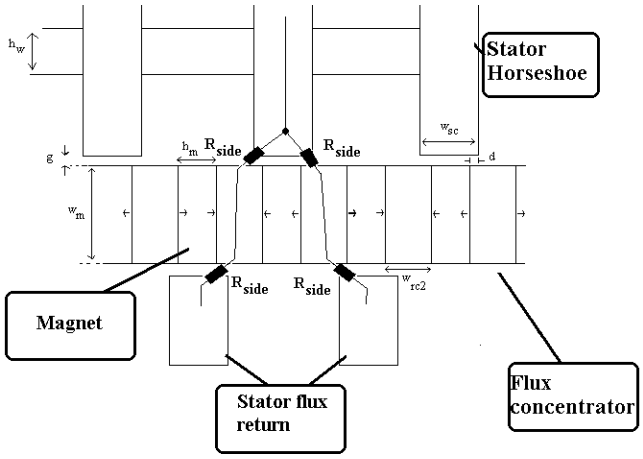


Fig. 6. Side view of the TFPM machine with flux concentration and double-sided air gap, shown in the unaligned position. Only one side of the rotor is shown.

The reluctance $R_{up}$ is then equal to:

$$R_{up} = 2R_{side} \tag{14}$$

To calculate the value of the lumped reluctances $R_m$, $R_{Ccore}$, $R_{SScore}$, $R_{LEC}$, $R_{ctc}$, $R_g$, $R_{side}$, and the mmf $F_m$, we use (15) - (22). Equations (19)-(22) are derived from the collection of a high number of 3-D finite element computations.

$$R_m = \frac{h_m}{\mu_0 \mu_{rm} w_m l_f} \tag{15}$$

$$F_m = \frac{h_m B_r}{\mu_0 \mu_{rm}} \tag{16}$$

$$R_{Ccore} = \frac{l_{sw} + 2h_{sw} + (2\sqrt{2}+1)l_f}{\mu_0 \mu_{rFe} w_{sc} l_f} \tag{17}$$

$$R_{SScore} = \frac{l_{sw} + \sqrt{2}h_{sw} - 2l_f}{\mu_0 \mu_{rFe} w_{sc} l_f} \tag{18}$$

$$R_{LEC} = \frac{h_m}{\mu_0 w_m}\left(0.66 - 0.073 h_m + 2.6\times10^{-3} h_m^2 + \frac{0.012 w_{rc2} + 0.037 w_m}{h_m}\right) \tag{19}$$

$$R_{ctc} = \frac{1}{\mu_0 l_f}\left[0.63 - 0.060\frac{w_{sc}}{w_{rc2}} + 0.060\frac{w_{sc}^2}{w_{rc2}^2} + 0.21\frac{h_m}{w_{rc2}} + 0.082\frac{h_m^2}{w_{rc2}^2}\right] \tag{20}$$

(21)

$$R_g = \frac{g}{\mu_0 l_f w_{rc2}}\left[1.3 - 0.64\frac{w_{sc}}{w_{rc2}} + 0.17\frac{w_{sc}^2}{w_{rc2}^2} + 0.028\frac{w_{rc2}}{g} - 6.4\times10^{-4}\frac{w_{rc2}^2}{g} - 2.3\frac{g}{l_f} + 3.8\frac{g^2}{l_f^2}\right]$$

$$R_{side} = \frac{g}{\mu_0 l_f w_{rc2}}\left[1.6 + 0.49\frac{d}{g} - 0.93\frac{d}{w_{rc2}} - 1.04\frac{w_{sc}}{w_{rc2}} + 0.16\frac{w_{sc}}{g}\right] \tag{22}$$

The torque of the TFPM machine can be predicted from (8), if the maximum available magnetomotive force $F_s$ is known. The maximum value of $F_s$ is $F_{smax}$, which is determined from the expression of the flux $\Phi_{ps}(t)$ created by the stator winding in the core of a salient TFPM machine.

$$\Phi_{ps}(t) = \frac{F_s}{4}\left(\sin\theta\left[\left(\frac{1}{R_{up}} + \frac{3}{R_{ap}}\right)\cos\omega t + \left(\frac{1}{R_{up}} - \frac{1}{R_{ap}}\right)\cos 3\omega t\right]\right) + \ldots$$

$$\ldots\frac{F_s}{4}\left(\cos\theta\left[\left(\frac{1}{R_{up}} + \frac{3}{R_{ap}}\right)\sin\omega t + \left(\frac{1}{R_{up}} - \frac{1}{R_{ap}}\right)\sin 3\omega t\right]\right) \tag{23}$$

The total flux can be written:

$$\Phi_{ptot}(t) = \Phi_{ps}(t) + \Phi_{pnl}\cos(\varpi t - \pi) \tag{24}$$

The value of $F_{smax}$ is limited by the saturation flux density $B_{Fesat}$ in the stator core, due to the sum of $\Phi_{pnl}(t)$, and $\Phi_{ps}(t)$. The saturation flux is defined as:

$$\Phi_{psat} = B_{Fesat} w_{sc} l_f \tag{25}$$

To obtain $F_{smax}$, we vary $\omega t$ by software, between *0* and $2\pi$, and set $\Phi_{ptot}$ to its saturation flux $\Phi_{psat}$ defined by (25). Using (23) and (24), we can determine a certain value of $\omega t$ for which $F_s$ is maximum. This is the value we use for $F_{smax}$.

In the calculations, the following values are used:

- $J$ = 5.0 A/mm2
- $k_{sfill}$ = 0.5
- $B_r$ = 1.23 T
- $\mu_{rFe}$ = 1000
- $\mu_{rm}$ = 1.09
- $B_{FEsat}$ = 1.9 T
- $\theta$ = 0 degree

## V. Performance of TFPM and RFPM machines with increasing air gaps

Using the models developed in the last section, the two programs vary all geometrical parameters, and calculate the corresponding torque. The programs use the geometrical parameters to calculate the machine mass and cost. The programs retain the lowest value of the cost/torque ratio. In the case of the TFPM machine, the optimal design is also verified by implementing the resulting geometry in a 3-D finite element analysis (FEA) package. The torque obtained with the mathematical model is compared with the torque obtained with FEA as a validation tool.

Optimal designs of the RFPM and TFPM machines are calculated for diameters varying between 0.5 m and 4 m, and for air gap thickness varying between 0.5 mm and 4 mm. The resulting cost/torque are presented in fig. 7 and fig. 8.

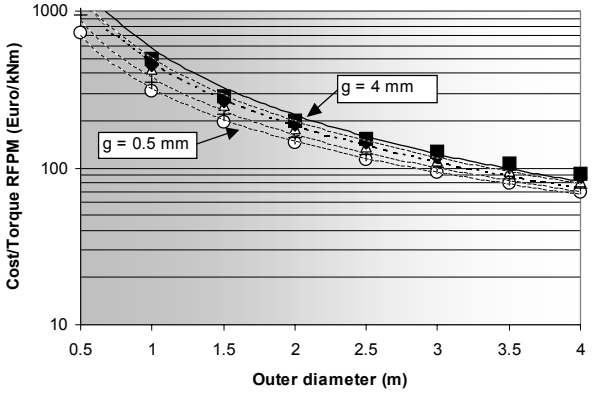


Fig. 7. Cost / Torque ratios of optimized RFPM machines as a function of diameters and air gap thickness. Air gap values: 0.5 mm , 1 mm , 2 mm , 3 mm , 4 mm.

Inspection of fig. 7 indicates only little influence of the air gap thickness on the RFPM cost/torque, while the cost/torque of the TFPM machine (fig. 8) is very sensitive to air gap thickness variation. It must be noted that the optimization process targetted machine designs with similar efficiencies (fixed to 92% in this case). The efficiency has an influence on the cost/torque, which has not been analyzed in the paper.

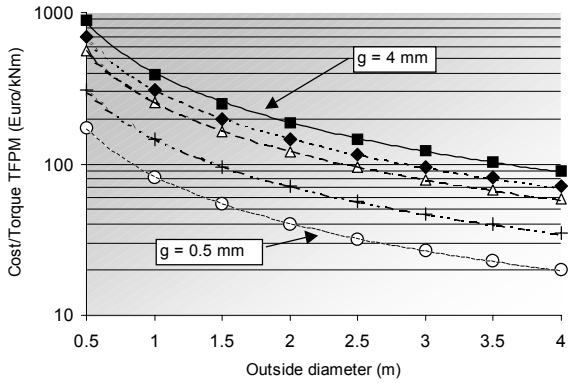


Fig. 8. Cost / Torque ratios of optimized TFPM machines as a function of diameters and air gap thickness. Air gap values: 0.5 mm , 1 mm , 2 mm , 3 mm , 4 mm.

Fig. 9 shows the TFPM cost advantage factor $K_{TFPM\_Cost}$, as defined by (26).

$$K_{TFPM\_Cost} = \frac{Cost\,/\,Torque - RFPM}{Cost\,/\,Torque - TFPM} \tag{26}$$

Fig. 9 shows that the TFPM machine with flux-concentration provides a significant cost advantage in active material, over the RFPM machine, for an air gap of 0.5 mm. However, this advantage is reduced when the air gap increases.

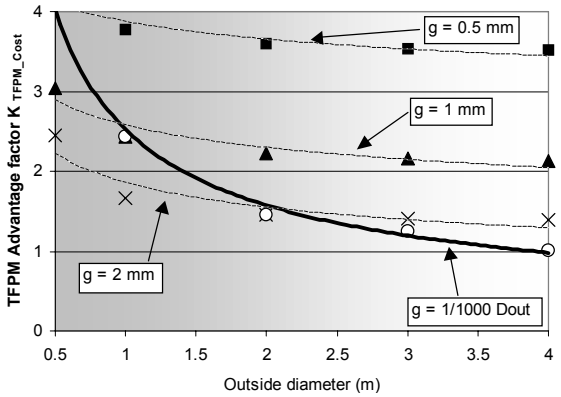


Fig. 9. Cost advantage factor of the TFPM machine over the RFPM machine. Square = air gap 0. 5 mm, Triangle = 1 mm, Cross = 2 mm, Circle = 1/1000 of outside diameter.

In direct-drive wind turbines, the TFPM machine with flux-concentration is a good choice to reduce the cost of active material. However, the air gap thickness should be maintained below 3 mm, in order to provide a good cost advantage. Fig. 8 also indicates that increasing the diameter also reduces the cost of active material. An interesting combination for cost reduction would be to use a TFPM machine with flux-concentration, with a large diameter and a thin air gap. However, mechanical considerations may prevent such a combination to be feasible. If the common practice of using an air gap of $1/1000^{th}$ of the machine outer diameter is used, then the two machine types give comparable cost/torque performances when used with a 4-meter diameter. Above that point, we observe that TFPM machine with flux-concentration is no longer an interesting choice.

## VI. Causes of TFPM sensitivity to air gap thickness

The great strength of the TFPM machine is to allow a lot of freedom on the pole pitch value. To make the no-load voltage as high as possible, a short pole pitch is normally selected. The drawback of having short pole pitches is the presence of strong leakage paths, which in the TFPM machine investigated here take place between adjacent flux concentrators.

The increase in air gap thickness increases the air gap reluctance $R_g$, without changing the reluctance $R_{LEC}$ and $R_{ctc}$ of the leakage paths. The no-load flux density in the stator core will be strongly reduced by an increasing value of $R_g$. High levels of no-load flux density can be maintained only by:

- increasing the magnet thickness $h_m$
- increasing the magnet width $w_m$

In both cases, the saturation flux density of the flux concentrators becomes a limiting factor. The increase in magnet thickness or width forces the designer to increase the width of the flux concentrator, in the order to avoid saturation. In all cases, the result of an increase in air gap thickness is an increase in pole pitch. Fig. 10 shows the pole pitch obtained from the optimization programs for the TFPM machine with flux concentration and double-sided air gap. The pole pitch is given as a function of the air gap thickness.

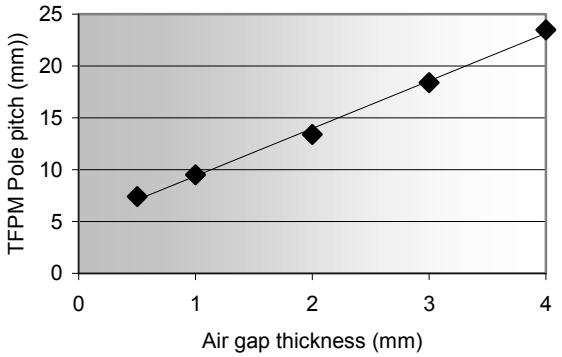


Fig. 10. Pole pitch of the TFPM machine with flux concentration as a function of air gap thickness. The pole pitch is chosen for a design with the minimum cost/torque. The flux concentrators are made of powdered iron, and have a saturation flux density of 1.6 T.

While a 1-mm air gap favors TFPM designs with pole pitches below 10 mm, a 4-mm air gap will favor TFPM designs with pole pitches around 25 mm. According to (8), a

same torque is obtained, if the decrease in the number of poles is compensated by an increase in the maximum mmf, and an increase in the no-load flux density. The increase in maximum mmf also increases the winding window area, the mass of copper winding and the size of the stator cores. Thus, the thicker the air gap thickness, the higher the mass of PM material, copper and iron required for a given torque.

## VII. CONCLUSION

The cost/torque characteristics of TFPM machines with flux concentration and RFPM machines have been investigated. Analytical models have been developed for both machine types. Optimization programs have been developed, allowing the prediction of designs with the lowest cost/torque.

The results of the optimization process are obtained for machine diameters between 0.5 m and 4 m and for air gap thickness of 0.5 mm and 4 mm. The cost/torque of the RFPM machine shows very little dependency on the air gap thickness, while the TFPM machine with flux concentration shows a strong dependency. The TFPM machine with flux concentration shows a cost advantage factor of about 3.5 with an air gap thickness of 0.5 mm. The cost advantage factor decreases to about 1 as the air gap thickness increases to 4 mm. Direct-drive wind turbine generators can benefit from a TFPM machine with a large diameters and a thin air gap. But in that case, further attention should be given to the mechanical design of such machines.

## VIII. REFERENCES


[1] "Wind energy – The Facts.", European Wind Energy Association, Brussels, Belgium, 1999

[2] D. Millborow, "Looking More Competitive than Ever," *WindPower Monthly*, pp. 32-33, Jan. 2001.

[3] G. Böhmeke, R. Boldt, H. Beneke, "Direct Drive, Geared Drive, Intermediate Solutions – Comparison of Design Features and Operating Economics," in *Proc. 1997 European Wind Energy Conf*, pp. 664-667.

[4] T. Hartkopf, M. Hofmann and S. Jöckel, "Direct-Drive Generators for Megawatt Wind Turbines," in *Proc. 1997 European Wind Energy Conf.,* pp. 668-671.

[5] S. Jöckel, "Gearless Wind Energy Converters with Permanent Magnet Generators- An Option for the Future?," in *Proc. 1996 European Union Wind Energy Conf.,* pp. 414-417.

[6] H. Weh, "Permanentmagneterregte Synchronmaschinen hoher Kraftdichte nach dem Transversalflusskonzept," *etzArchiv*, vol. 10, pp. 143-149, 1988.

[7] G. H. Pajooman, "Performance Assessment and Design Optimisation of VRPM (Transverse Flux) Machines by Finite Element Computation," Ph.D. dissertation, Dept. Elect. Eng., Univ. Southampton, England, 1997.

[8] G. Henneberger and R. Blissenbach, "Transverse Flux Motor with High Specific Torque and Efficiency for a Direct Drive of an Electric Vehicle," in *Proc. 1999 Clean Power Sources and Environmental Implications in the Automotive Industry Conf.*, Vienna, Austria, pp. 429-436.

[9] A. Grauers, "Design of Direct-driven Permanent-magnet Generators for Wind Turbines," Ph.D. dissertation, School Elect. and Computer Eng., Chalmers Univ. Tech., Göteborg, Sweden, 1996.


## IX. BIOGRAPHIES

**Maxime R. Dubois** was born in Alma, Québec, Canada, in 1968. He received the B. Ing. and M. Sc. degrees in 1991 and 1993, both in Electrical Engineering from the Université Laval, Québec, Canada,. Between 1993 and 1999, he worked as a design engineer for private companies in Canada, in the area of power electronics. Since 1999, he is with the Laboratory of Electrical Power Processing of Delft University of Technology, in The Netherlands, and is heading towards a Ph.D. degree.
His main interests are machines and power electronics applied to the generation of energy from renewable sources.

**Dr. Henk Polinder** was born in Nunspeet, the Netherlands in 1968. He received his M.Sc. degree in 1992 and his PhD degree in 1998 both in electrical engineering at Delft University of Technology, The Netherlands. Currently, he is an assistant professor at the Electrical Power Processing Laboratory at the same university, where he gives courses on electrical machines and drives. His research interests are in the field of electromechanical power conversion.
He works on e.g. direct drive generators for wind turbines, linear direct drive generators for wave energy and actuators for high precision motion control.

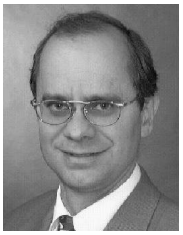

**Dr. J.A. Ferreira** was born in Pretoria, South Africa, and received the B.Sc.Eng.(cum laude), M.Sc..Eng.(cum laude), and Ph.D. degrees in Electrical Engineering from the Rand Afrikaans University, Johannesburg, South Africa, in 1980, 1982, and 1988, respectively.

In 1981 he was with the Institute of Power Electronics and Electric Drives, Technical University of Aachen, and worked in industry at ESD(Pty) Ltd from 1982-1985. From 1986 until 1997 he was at the Faculty of Engineering, Rand Afrikaans University, where he held the Carl and Emily Fuchs Chair of Power Electronics. Since 1998 he is professor at the ITS Faculty of the Delft University of Technology in The Netherlands

Prof. Ferreira is the transactions review chairman of the IEEE IAS Power Electronic Devices and Components committee, vice-chairman of the IEEE Joint IAS/PELS Benelux chapter and chairman of the CIGRE SC14 national committee of the Netherlands. He is also member of the IEEE PESC Adcom, and member of the executive committee of the EPE Society.